Morphology Detection for Magnetically Self-Assembled Modular Robots

Zoltán Nagy, Shuhei Miyashita, Simon Muntwyler, Ashish K. Cherukuri, Jake J. Abbott,
Rolf Pfeifer, and Bradley J. Nelson

Abstract—**Self-assembly is a process in which individual components form an organized structure as a consequence of local interactions. When using magnetics to create interaction forces, the magnetic flux distribution of a self-assembling system changes as its assembly state varies. Since Hall effect sensors are a convenient and effective means to detect changes in the magnetic field, we explore their applicability to monitoring the morphology of such magnetically self-assembling systems. We find that optimal positions for the sensor can be found where the flux changes maximally. Our analysis is applied to two different systems by deriving the flux changes for all possible states, and theoretical flux changes are verified with experiments. In addition, we show that a small number of sensors is sufficient for robust state determination. In addition to state detection, experiments show the potential for angle measurement for compliant cylindrical magnet joints using a single Hall sensor.**

I. Introduction

Self-assembly is the organization of individual components into regular structures without a global control scheme. Self-assembly occurs from the molecular to the planetary scale [1], and current research focuses on the creation of self-replicating, self-organizing, or self-reconfigurable robotic systems as artifical instantiations of self-assembly [2]–[4].

To study self-assembling systems at the cm scale, it is convenient to use magnets to provide sufficient interaction forces and torques, and thus motion, without the need for additional power. Magnetic interaction has been shown to scale favorably to the micro and nanodomain, implying that knowledge gained at the cm-scale will translate well to the sub-mm domain [5].

The morphology, i.e. the shape, of a magnetically self-assembled system is not only characterized by its geometrical boundary, but also by the distribution of the magnetic field—as the shape of the system changes, so does the magnetic field distribution. If this change is unique, then knowledge of the field variation leads to knowledge of the morphology variation. In this paper, we numerically and experimentally investigate the existence of such unique mappings for two different situations: detection of individual self-assembly states, i.e. online monitoring of the stochastic self-assembly process, and determination of the relative position of the modules separated by compliant joints.
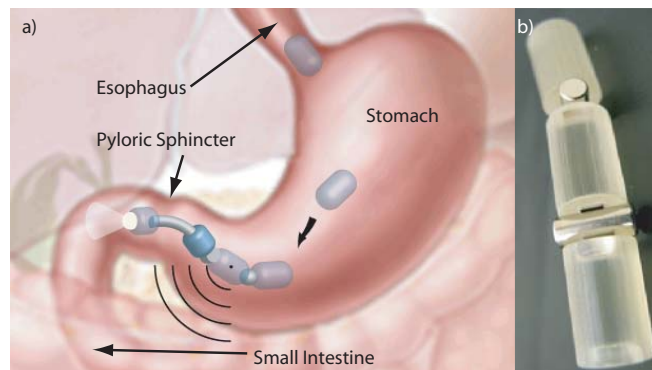
Fig. 1. a) Concept drawing for a swallowable self-assembling modular robot. b) Snake-type robot with simple prototype modules, which is assembled in a plastic stomach in [6].
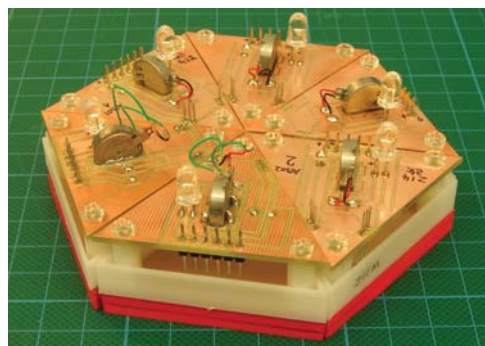

Fig. 2. Tribolon system used to study self-assembly at the cm-scale.

In [6], [7] the concept for a swallowable modular robot for medical interventions was introduced, together with statistical results on self-assembling cylindrical modules with different magnet configurations at the ends (see Fig. 1a)). It was shown that succesful self-assembly can be achieved, provided that the magnetization of the magnet lies in the plane of the mating face (MASH-1 configuration). In addition to the successfully assembled state, locally stable misaligned states have been identified. In Section III-A we show numerically and experimentally the existence of a sensor location enabling identification of each of these states.

In [8], [9] the stochastically self-assembling Tribolon system was introduced. It consists of triangular modules floating on water and eventually assembling into a final, hexagonal configuration (see Fig. 2). The modules feature one magnet providing the intermodular attraction force, and a vibration motor generating a random motion component. The assembly of the final hexagonal configuration is known

to be affected by the so-called yield problem, where clusters of either 4 or 5 modules cannot attach together and remain as "garbage" [10]. One proposed solution is implementing graph grammar rules to the modules, allowing them to communicate with each other in order to decide whether they should remain connected or not. [3]. This method makes the process of assembly into particular morphologies predictable and programmable. Another solution is based on low-level control in which case the formation of the clusters is restricted to a maximum of three modules and only such clusters can attach to one another. Our goal here is to achieve this end without the need for intermodular communication. This requires that the global information of the cluster size is available to each module locally. In Section III-B we propose a solution that allows a given module to detect its state transitions, and thus the size of the cluster it is in, and demonstrate simple behavior with three modules.

Hall effect sensors are often used to measure magnetic fields. The main advantage of these devices over, for example, optical sensing methods is that they can be completely sealed and used in harsh environments. Hall sensors are widely used in position and orientation sensing applications, and, in this work, we are interested in their applicability to the detection of self-assembly states. However, preliminary experiments show that we can also use the same sensors in a more traditional way, namely as joint-angle sensors in situations like the one depicted in Fig. 1b), where the joints between the modules in the snake-type system are diametrically polarized cylindrical magnets allowing for one degree of freedom rotation of the modules with respect to each other [6]. This is discussed in section IV.

II. DETECTING CHANGES IN MAGNETIC FIELDS

The output voltage of the Hall effect sensor we use in our experiments (A1302 from Allegro Microsystems Inc.) is proportional to the magnetic flux density across it. In particular, the change in voltage ΔV is related to the flux change $|\Delta \mathbf{B}|$ through the sensitivity $S = 13\text{mV/mT}$ of the sensor as $\Delta V = S|\Delta \mathbf{B}|$. The Hall sensors are interfaced to a PC using a National Instruments USB-6008 data acquisition card and LabView.

We are interested in using as few sensors as possible to determine the required information. Therefore, we numerically determine the optimal position of the Hall sensor for a given problem. This optimal position is characterized by the largest change in the magnetic flux as the system changes from one morphology to another and, thus, allows for the least ambiguous sensing of the state transition.

For the numerical optimization, the magnetic field of the magnets is computed using the surface charge models provided in [11] and partially reproduced in the Appendix. These equations can be used to determine the field of nearby multipole structures, and are computationally effective as no discretization of the space is necessary (as opposed to finite-element-based methods). When the inter-magnet distance is much larger than the magnet size, a simple point-dipole model is sufficient.

We begin by a qualitative analysis of the flux change. Let $\mathbf{B}_{\mathcal{S}_1}$ and $\mathbf{B}_{\mathcal{S}_2}$ be the flux distributions of a first shape $\mathcal{S}_1$ and a second shape $\mathcal{S}_2$, respectively. Then, for an arbitrary reference frame j

$$\mathbf{B}_{\mathcal{S}_1}^{\mathbf{j}}(\mathbf{x}^{\mathbf{j}}) = \sum_{i=1}^{n} g_{ji}\mathbf{B}^{\mathbf{i}}(\mathbf{x}^{\mathbf{i}}) = \sum_{i=1}^{n} g_{ji}\mathbf{B}^{\mathbf{i}}(g_{ij}\mathbf{x}^{\mathbf{j}}), \text{ and}$$

$$\mathbf{B}_{\mathcal{S}_2}^{\mathbf{j}}(\mathbf{x}^{\mathbf{j}}) = \sum_{i=1}^{n+m} g_{ji}\mathbf{B}^{\mathbf{i}}(\mathbf{x}^{\mathbf{i}}) = \sum_{i=1}^{n+m} g_{ji}\mathbf{B}^{\mathbf{i}}(g_{ij}\mathbf{x}^{\mathbf{j}})$$

where $\mathbf{x}^{\mathbf{j}} \in \mathbb{R}^3$ is the point where we are computing the field, expressed in the frame j, $\mathbf{B}^{\mathbf{i}}$ is the field of magnet i in its own frame i, g_{ji} is the homogeneous transformation from frame i to frame j, with $g_{ij} = g_{ji}^{-1}$, n is the number of magnets in the first shape, and m is the number of additional magnets in the second shape. The flux change at $\mathbf{x}^{\mathbf{j}}$ follows as

$$\Delta \mathbf{B}^{\mathbf{j}}(\mathbf{x}^{\mathbf{j}}) = \mathbf{B}_{\mathcal{S}_2}^{\mathbf{j}}(\mathbf{x}^{\mathbf{j}}) - \mathbf{B}_{\mathcal{S}_1}^{\mathbf{j}}(\mathbf{x}^{\mathbf{j}}) = \sum_{i=n+1}^{n+m} g_{ji}\mathbf{B}^{\mathbf{i}}(g_{ij}\mathbf{x}^{\mathbf{j}}) \quad (1)$$

That is, the flux change is simply equal to the flux of the additionally introduced magnets. In the simplest case ($n = m = 1$), $\mathbf{B_1}$ is provided by a single magnet on a given module, and $\Delta \mathbf{B}$ by a second magnet on another module. Thus, to optimally detect the presence of the second module with sensors inside the first module, the position of the maximal flux due to the second module's magnet occuring inside the first module is required. This position is close to the second magnet as the magnetic flux generally decreases with distance from a magnet. We conclude that the optimal position is near the boundary of the first module.

For the numerical analysis, the field equations are implemented in MATLAB and used in the numerical maximization of the flux change between two morphologies as follows. We choose $j = 1$, i.e. we express the fields in the frame of magnet 1 and omit the superscript from now on. We identify the different occuring shapes $\mathcal{S}$ and derive the transformations g_{1i}. Then, we use MATLAB's fmincon to solve the optimization problem in each component B_i of $\mathbf{B}$

$$\begin{aligned} \text{minimize} \quad & -\Delta B_i \\ \text{subject to} \quad & \mathbf{x} \in \mathcal{C}, \end{aligned} \quad (2)$$

and designate the optimal position as $\mathbf{x}^\star$, $\mathcal{C}$ designates the feasible region for $\mathbf{x}^\star$—that is, the region where we could realistically place a Hall effect sensor. Considering the individual components in the optimization process, rather than the norm $|\Delta \mathbf{B}|$, also considers situations where $\mathbf{B}$ rotates while its magnitude remains constant. Additionally, if the optimal position for two components i and j is the same, an optimal orientation of the Hall sensor can be derived as $\theta = \arctan(\Delta B_i / \Delta B_j)$.

III. MORPHOLOGY DETECTION

A. Swallowable Modular Robot

Figure 3 shows the observed self-assembly states from [6]. The success rate ('S') was found to be $> 70\%$ when using

TABLE I

OPTIMAL LOCATIONS AND THE CORRESPONDING MAXIMAL FLUX CHANGES VERSUS THE UNCONNECTED STATE ($\mathcal{S}_1$) GIVEN THE HALL EFFECT
SENSOR CAPTURING THE FLUX IN THE PRINCIPLE DIRECTIONS.

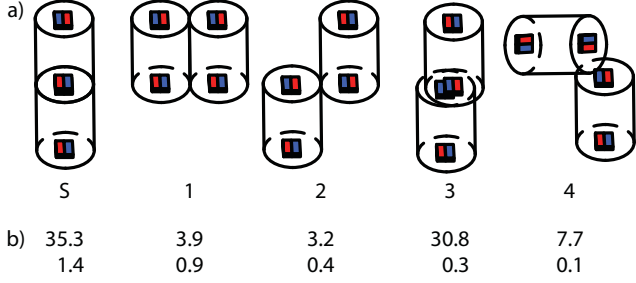| State	x-direction		y-direction		z-direction	
$\mathcal{S}_2$	$\mathbf{x}^\star$ [mm]	$|\Delta B_x|$ [mT]	$\mathbf{x}^\star$ [mm]	$|\Delta B_y|$ [mT]	$\mathbf{x}^\star$ [mm]	$|\Delta B_z|$ [mT]
S	[2.8,-2.0,2.8]	8.6	[0,-1.5,2.4]	35.3	[0,-2.0,0]	27.5
1	[2.1,-2.0,-4.0]	7.2	[0,-2.5,-4.5]	14.9	[0,-2.0,-4.5]	21.1
2	[2.1,-2.0,-4.0]	7.2	[0,-2.5,-4.5]	14.2	[0,-2.0,-4.5]	21.0
3	[-0.7,-2.0,2.2]	1.3	[0.8,-1.5,0.4]	19.7	[0,-2.0,-4.0]	27.5
4	[-3.1,-2.0,3.3]	2.3	[0,-1.5,3.3]	8.3	[0.1,-2.0,0]	7.2

Fig. 3.   a) Self-assembly states of the abstract swallowable modular robot system [6]. b) Flux change results for sensors placed at $\mathbf{x_2}^\star$ at each end of the module (see Fig. 4). Clearly, each state can be identified uniquely.
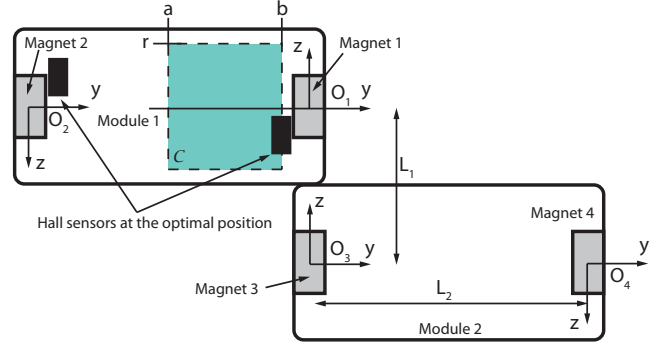

Fig. 4.   Coordinate frames for state 2, a, b, r represent the cylinder in which we search the optimal location, the distances L_1 and L_2 are measured from the magnet center. The hall sensors are shown at $\mathbf{x_2}^\star$ for magnet 1 and its equivalent position for magnet 2 (see text).

$4 \times 4 \times 2\text{mm}^3$ magnets with $B_r = 1.4$T remanance. Using the same magnets, we wish to determine how many Hall sensors are needed as well as their optimal positions to detect each of these states uniquely.

We consider modules with length 20mm and diameter 10mm with an anti-parallel magnet configuration, i.e. the magnets on a given module are oriented in opposite directions as shown in Fig. 3. We define as $\mathcal{S}_1$ the unconnected state (one module with two magnets $\mathbf{B^1}$ and $\mathbf{B^2}$), and $\mathcal{S}_2$ as one of the states in Fig. 3 (one additional module with magnets $\mathbf{B^3}$ and $\mathbf{B^4}$). According to (1), the flux change expressed in the frame of magnet 1 is

$$\Delta \mathbf{B} = \sum_{i=3}^{4} g_{1i} \mathbf{B^i} \tag{3}$$

Let us consider Fig. 4 as an example for $\mathcal{S}_2$. The homogeneous transformations g_{13} and g_{14} are given by

$$g_{13} = \begin{bmatrix} & & & 0 \\ & \mathbf{I}_{3\times3} & & 0 \\ & & & -L_1 \\ & \mathbf{0}_{1\times3} & & 1 \end{bmatrix}, \ g_{14} = \begin{bmatrix} -1 & 0 & 0 & 0 \\ 0 & 1 & 0 & L_1 \\ 0 & 0 & -1 & -L_2 \\ 0 & 0 & 0 & 1 \end{bmatrix}.$$

The coordinate frames are centered in the magnets' centers, such that the magnetization of the magnet is along the positive z-axis, the y-axis is chosen the same for each magnet for simplicity, and the x-axis is such that a right-handed orthonormal base is obtained. Following our argument of the previous section, the maximal flux change will occur where magnets 3 and 4 introduce a combined maximal flux into module 1. We constrain the feasible region to a cylindrical space behind magnet 1:

$$\mathcal{C} = \left\{ (x, y, z) \, \middle| \, x^2 + z^2 - r^2 \leq 0 \text{ and } a \leq y \leq b \right\}, \tag{4}$$

with $r = 4.5$mm, $a = -10$mm, $b = y_{\max}$, and $y_{\max} = -1.5$mm when the Hall device is sensing in the y-direction and $y_{\max} = -2.0$mm when the sensor measures in the z-direction—this takes into account the position of the effective Hall probe inside the SIP-3 package.

The optimal locations $\mathbf{x}^\star$ for each component B_i are shown in Table I. We observe that in the x-direction the maximal flux changes are comparatively low. As for $\mathbf{x}^\star$, two interesting positions can be identified. First, the success state is detected best at $\mathbf{x}^\star = [0, -1.5, 2.4]$mm in the y-direction or with similar flux change at $\mathbf{x}^\star = [0, -2, 0]$mm in the z-direction. Second, the optimal positions when measuring the flux in the z-direction for states 1–3 are relatively close together. We conclude from Table I that it is possible to uniquely detect each occuring state.

However, requiring optimality for each state necessitates the use of multiple sensors. Since it is desirable to use as few sensors as possible, we proceed to investigate the flux change at specific locations based on the previous result: the absolute best position for detecting the success state $\mathbf{x_1^\star} = [0, -1.5, 2.4]$mm, its symmetrical counterpart $\mathbf{x_2^\star} = [0, -1.5, -2.4]$mm, both measuring the flux in y-direction, and at $\mathbf{x_3^\star} = [0, -2, -4.5]$mm and $\mathbf{x_4^\star} = [0, -2, 4.5]$mm, measuring the flux in z-direction. We conclude from the results in Table II that each of these positions allows us to uniquely identify the states. And even though states 1 and 2 show similar flux changes, they are easily distinguished with a second Hall sensor close to magnet 2, which will already be available in order to detect the connection states on the second face.

TABLE II

FLUX CHANGE (IN MT) FOR THE STATES AT $\mathbf{x_1^\star} - \mathbf{x_4^\star}$ (SEE TEXT). WE OBSERVE THAT EACH OF THESE LOCATIONS ALLOWS FOR THE DISTINCTION OF THE STATES.

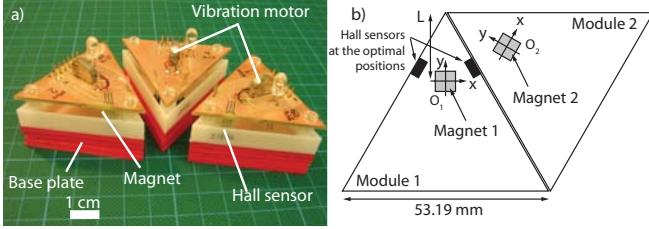| States	$|\Delta B_y|$ at $\mathbf{x_1^\star}$	$|\Delta B_y|$ at $\mathbf{x_2^\star}$	$|\Delta B_z|$ at $\mathbf{x_3^\star}$	$|\Delta B_z|$ at $\mathbf{x_4^\star}$
S	35.3	35.3	5.9	5.9
1	0.9	3.9	21.1	1.5
2	0.2	3.2	21.0	1.6
3	8.6	30.8	26.5	4.5
4	7.7	7.7	0.3	0.3

Fig. 5. Tribolon modules. a) Photo, b) Employed coordinate frames.

For experimental verification, cylindrical modules were fabricated by stereolithography and the magnets were glued into the faces. One Hall sensor was glued behind the magnet at $\mathbf{x_2^\star}$ and connected to the data acquisition system. The output voltages for each state are recorded and the difference to the unconnected state is determined. Finally, we convert the voltage difference to flux change and find $|\Delta B_y| = \{37.6, 5.8, 5.0, 34.1, 14.6\}$mT for the states S–4, which corresponds well with the theoretical results in Table II.

Finally, we compute the flux changes for a potential application by assuming two hall sensors inside Module 1 at $\mathbf{x_2^\star}$ and the equivalent position for Magnet 2 as shown in Fig. 4. The results, shown in Fig. 3b), show again that unique flux changes are obtained, and thus the states are identifiable.

We conclude that a single Hall sensor at each magnet is sufficient to detect all the occuring states of the self-assembly process. In addition, equivalent locations exist where an additional Hall sensor can be used to increase the robustness of the detection procedure and/or provide design alternatives.

B. Tribolons

Self-assembling systems at the cm scale are typically considered as distributed systems, implying that there are uncertainties in the knowledge of the components' global information. Due to the lack of a central controlling system to coordinate and control the modules, each module is required to possess any necessary information of the global configuration. Fig. 5a) shows the Tribolon modules employed in this work. The modules are equilateral triangles (see Fig. 5b)), and the magnet ($B_r = 1.4$T) providing the attraction force between them is a cube of 5mm sidelength magnetized along the x-axis (perpendicular to the symmetry axis) and placed at $L = 15$mm from the tip of the module.

The morphologies that may occur during the self-assembly process are depicted in Fig. 6. We wish to determine the
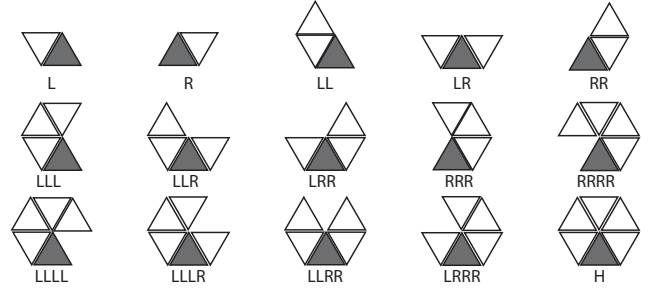

Fig. 6. Possible morphologies that may occur during the Tribolon self-assembly process. The nomenclature reflects the number of (L)eft and (R)ight neighbors of the gray module, and H designates the self-assembled hexagon.

number and position of the Hall sensors to enable a given module to sense the size of the cluster it is in, i.e. know how many left and right neighbors it has. We begin by determining the optimal position to detect one neighbor—the situation depicted in Fig. 5b)—and define $\mathcal{S}_1$ as the state without any neighbor, and $\mathcal{S}_2$ as the state with one right neighbor (R). Then,

$$g_{12} = \begin{bmatrix} 1/2 & -\sqrt{3}/2 & 0 & \sqrt{3}L/2 \\ \sqrt{3}/2 & 1/2 & 0 & L/2 \\ 0 & 0 & 1 & 0 \\ 0 & 0 & 0 & 1 \end{bmatrix}. \quad (5)$$

With the feasible region $\mathcal{C}$ being the whole module 1 except the position of the magnet, and $x_0 = [4, 4, 0]$mm, we find the optimal position to be at $\mathbf{x^\star} = [2.6, 9.8, 0]$mm, which is at the boundary of the module. Also, we find that the change of both flux components ΔB_x and ΔB_y is maximal at this position, therefore, the Hall sensor should be oriented to capture the flux at the angle $\arctan(\Delta B_y/\Delta B_x) = \pi/6$ (perpendicular to the wall of the module).

We also find that the flux change at the symmetric position $\mathbf{x_2^\star} = [2.6, -9.8, 0]$ is negligible, therefore, it can be used to optimally detect a (L)eft neighbour. Thus, we equip the modules with two Hall sensors at $\mathbf{x^\star}$ and $\mathbf{x_2^\star}$ and investigate this configuration for its utility in detecting state transitions. Fig. 7 shows the percentage change in the flux for both sensors for all possible state transitions (except for symmetry). We observe that every transition causes a flux change of at least 1% which can be detected with appropriate hardware. For robustness of detection, one could implement the possible transitions onto the module given a certain cluster size. Then, the number of possibe transitions is greatly reduced. Either way, we conclude that the information on the global shape and size of the cluster, as well as the position of a given module inside this cluster, can be made available locally on the module.

Experimentally, we investigate the yield problem introduced earlier. To constraint the size of the cluster to three modules, it is necessary that a given module detects the states L, R, LL, LR, and RR. To show this, we implemented the following simple rule on one module: run the vibration motor as long as the cluster size is 1 or 2, else stop it. Before
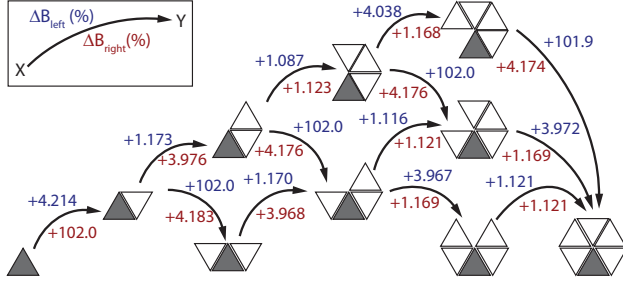
Fig. 7. Flux change (in %) for two optimally positioned Hall sensors on the gray module (see Fig. 5b)). Each state transition is unique and allows the gray module to monitor the size of the cluster.

TABLE III

VOLTAGE LIMITS FOR THE DIFFERENT TRIBOLON STATES

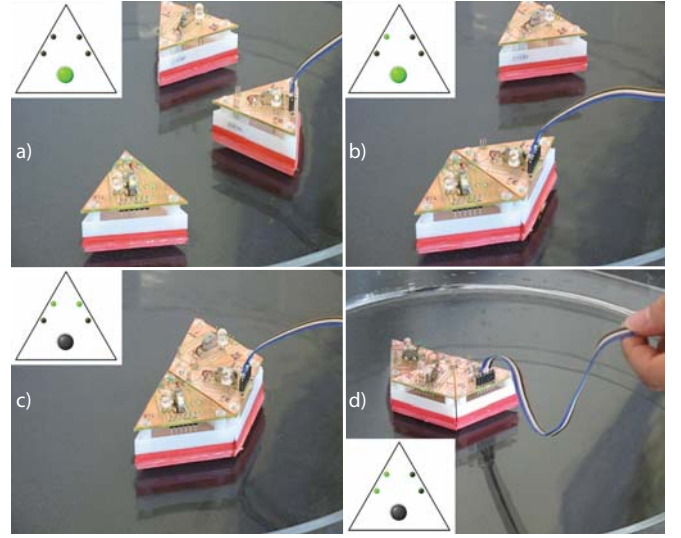| State	Left Sensor V_{max}	Left Sensor V_{min}	Right Sensor V_{max}	Right Sensor V_{min}
N	0.8	0.7	1.3	1.2
R	0.8	0.728	1.2	0.88
L	0.7	0.45	1.3	1.208
RR	0.8	0.7	0.873	0.85
LL	0.727	0.45	1.208	1.2
RL	0.8	0.43	0.879	0.8

Fig. 8. Example for Tribolon state transition. The inset indicates the state as seen by the active module during the experiment, and its action (small circles: dark (no neighbor) and bright (connected neighbor); large circle: dark (motor stopped) and bright (motor running)): a) no neighbor: motor running, b) L: motor running, c) RL: motor stopped, d) LL: motor stopped. (see Fig. 6)
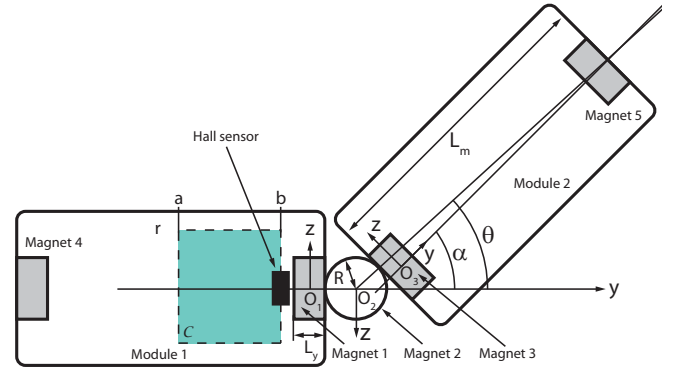
running the experiment we determined the voltage limits of the Hall sensors for the different states as shown in Table III. The sensor readout and the motor power supply was passed from and to the module by means of a cable, and the control was done in LabView. The other two modules were passive, i.e. their sensors and motor information was not processed. Snapshots of typical assembly states are shown in Fig. 8 together with the state of the module (a movie is provided as supporting material).

IV. JOINT ANGLE MEASUREMENT

When the modules assemble into a snake-type structure such as shown in Fig. 1b), they ideally line up as shown in Fig. 9, where the cylindrical magnet (magnet 2) is diametrically magnetized (i.e. bipolar cylindrical magnet). Now the modules can rotate with respect to each other and can, for example, adapt the shape of the robot to the walls of the intestine as they are moving through it. In this situation, our objective is to determine the angle between the modules, i.e. to use a Hall sensor as a wireless encoder for the passive cylindrical joint.

In the envisaged application, the cylindrical joint magnet will be rigidly attached (glued) to a given module, and allow another module without joint to self-assemble to it. We neglect the outer magnets 4 and 5, as they are relatively far away to have influence. We note that as Module 2 rotates on the cylindrical magnet, the center of rotation moves along the horizontal y axis. It follows that instead of the desired joint angle θ, we observe the angle α. Using trigonometric relationships we can relate α to θ as

$$\theta = \left(1 + \frac{L_m}{R}\right)\alpha, \qquad |\theta|, |\alpha| \leq \frac{\pi}{2} \qquad (6)$$

Fig. 9. Coordinate frames for joint angle measurement.

assuming that $L_m \gg R$, which holds in our case, as $L_m = 20$mm and $R = 2$mm. Similar to the previous section, we find the optimal position for various angles θ as $\mathbf{x}^\star = [0, -1.5, z^\star]$mm, where $z^\star$ is shown in the inset of Fig. 10. As can be seen, $z^\star$ is close to zero. For simplicity of alignment we choose $z^\star = 0$mm for the experiment, as now $x^\star$ is centered on the surface of the magnet. The optimal direction of the hall sensor is found to be the y-axis, that is the sensor should measure the flux perpendicular to the magnetization of the magnet.

Experimentally, we measure the flux change using a $5°$ angular grid fabricated out of PMMA with a laser mill. We set the two-module structure at the angles $\theta \in (0°, 55°)$ while the voltage was recorded. This was repeated six times. Finally, the difference to the $0°$ position is calculated. The results are shown in Fig. 10, together with a sinusoidial fit ($\Delta V = A \sin \theta$), and a linear fit ($\Delta V = C\theta$). We find $A = 0.1151$V with the 95% confidence interval $[0.1139, 0.1164]$V, and $C = 0.1038$V/rad with the
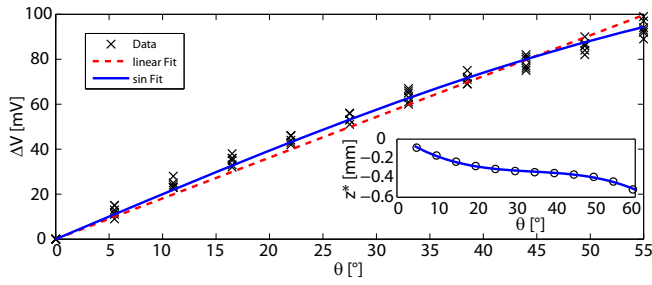
Fig. 10. Results for angle measurement with two fit functions. The inset shows the z-coordinate of the optimal location (model and cubic fit). For simplicity, $z^\star = 0$mm is chosen.

confidence interval $[0.1019, 0.1057]$V/rad. Good agreement is obtained between the sinusoidial fit and the model where we find $A = 0.130$V using the sensor's sensitivity $S = 13$mV/mT to convert between voltage and flux change.

We conclude that a single Hall sensor can be used as an encoder for the angle between two modules. Using $\theta = \arcsin(\Delta V/A)$, the measurement uncertainty $\Delta\theta$ for the angle detection can be calculated as

$$\Delta\theta = \frac{\partial\theta}{\partial\Delta V}\delta V = \frac{\delta V}{\sqrt{A^2 - \Delta V^2}}, \qquad (7)$$

where δV is the noise level of the Hall sensor. In our case ($\delta V = 0.1$mV), this results in $\Delta\theta < 1°$.

V. CONCLUSIONS & FUTURE WORK

Based on the premise that the flux distribution of a magnetically self-assembling system changes as its geometric shape changes, we have shown that linear Hall effect sensors can be used to uniquely identify the current state of the system. In addition, we have numerically derived optimal locations and orientations for the sensors for the maximal flux change. We have also demonstrated the efficiency of Hall sensors because the number of the necessary sensors for unique state detection can be very low. Specifically, in the case of the swallowable modular robot, only one sensor per magnet is necessary to detect all five occuring states, and for the Tribolons, only two sensors per module allow the distinction between sixteen shapes. This enables a given module to have local information on the global morphology of the cluster it is in. Finally, we have shown the potential for joint-angle measurements in self-assembled snake-type robots using a single Hall sensor, and found that the error on the measured angle can be as low as $1°$.

In addition to the examples presented in this work, our methodology is readily extended to virtually any system undergoing a flux distribution change upon shape change.

APPENDIX
SURFACE CHARGE MODELS

For a rectangular bar magnet with edge coordinates (x_1, x_2), (y_1, y_2), and (z_1, z_2), and magnetization $\mathbf{M} =$

$[0, 0, M_s]^T$ the **B**-field outside the magnet is given by

$$
\begin{aligned}
B_x(x, y, z) &= \frac{\mu_0 M_s}{4\pi} \sum_{k=1}^{2} \sum_{m=1}^{2} (-1)^{k+m} \\
&\quad \times \ln\left[F(x, y, z, x_m, y_1, y_2, z_k)\right] \\
B_y(x, y, z) &= \frac{\mu_0 M_s}{4\pi} \sum_{k=1}^{2} \sum_{m=1}^{2} (-1)^{k+m} \\
&\quad \times \ln\left[H(x, y, z, x_1, x_2, y_m, z_k)\right] \\
B_z(x, y, z) &= \frac{\mu_0 M_s}{4\pi} \sum_{k=1}^{2} \sum_{n=1}^{2} \sum_{m=1}^{2} (-1)^{k+n+m} \\
&\quad \times \arctan\left[\frac{(x - x_n)(y - y_m)}{(z - z_k)}\right. \\
&\quad \times \left. g(x, y, z, x_n, y_m, z_k)\right]
\end{aligned}
$$

with the remanence being $B_r = \mu_0 M_s$, and

$$
\begin{aligned}
F &= \frac{(y - y_1) + [(x - x_m)^2 + (y - y_1)^2 + (z - z_k)^2]^{1/2}}{(y - y_2) + [(x - x_m)^2 + (y - y_2)^2 + (z - z_k)^2]^{1/2}} \\
H &= \frac{(x - x_1) + [(x - x_1)^2 + (y - y_m)^2 + (z - z_k)^2]^{1/2}}{(x - x_2) + [(x - x_2)^2 + (y - y_m)^2 + (z - z_k)^2]^{1/2}} \\
g &= \frac{1}{[(x - x_n)^2 + (y - y_m)^2 + (z - z_k)^2]^{1/2}}
\end{aligned}
$$

More details on surface charge models can be found in [11].

REFERENCES

[1] G. M. Whitesides and B. Grzybowski, "Self-assembly at all scales," *Science*, vol. 295, no. 5564, pp. 2418–2421, 2002.
[2] S. Griffith, D. Goldwater, and J. M. Jacobson, "Robotics—self-replication from random parts," *Nature*, vol. 437, no. 7059, pp. 636–636, 2005.
[3] J. Bishop, S. Burden, E. Klavins, R. Kreisberg, W. Malone, N. Napp, and T. Nguyen, "Programmable parts: A demonstration of the grammatical approach to self-organization," in *Proc. IEEE/RSJ Int. Conf. Intelligent Robots and Systems*, 2005, pp. 3684–3691.
[4] P. J. White, K. Kopanski, and H. Lipson, "Stochastic self-reconfigurable cellular robotics," in *Proc. IEEE Int. Conf. Robot. Automat.*, vol. 3, 2004, pp. 2888–2893.
[5] O. Cugat, J. Delamare, and G. Reyne, "Magnetic micro-actuators and systems (MAGMAS)," *IEEE Trans. Magnetics*, vol. 39, no. 5, pp. 3607–3612, 2003.
[6] Z. Nagy, R. Oung, J. J. Abbott, and B. J. Nelson, "Experimental investigation of magnetic self-assembly for swallowable modular robots," in *Proc. IEEE/RSJ Int. Conf. Intelligent Robots and Systems*, 2008, pp. 1915–1920.
[7] Z. Nagy, K. Harada, M. Fluckiger, E. Susilo, R. Oung, I. K. Kaliakatsos, A. Menciassi, E. Hawkes, J. J. Abbott, P. Dario, and B. J. Nelson, "Assembling reconfigurable endoluminal surgical systems: Opportunities and challenges," *Int. J. Biomechatronics and Biomedical Robotics*, 2009, accepted.
[8] S. Miyashita, M. Kessler, and M. Lungarella, "How morphology affects self-assembly in a stochastic modular robot," in *Proc. IEEE Int. Conf. Robot. Automat.*, 2008, pp. 3533–3538.
[9] S. Miyashita, F. Casanova, M. Lungarella, and R. Pfeifer, "Peltier-based freeze-thaw connector for waterborne self-assembly systems," in *Proc. IEEE/RSJ Int. Conf. Intelligent Robots and Systems*, 2008, pp. 1325–1330.
[10] K. Hosokawa, I. Shimoyama, and H. Miura, "Dynamics of self-assembling systems: Analogy with chemical kinetics," *Artificial Life*, vol. 1, no. 4, pp. 413–427, 1994.
[11] E. P. Furlani, *Permanent Magnet and Electromechanical Devices.* San Diego, CA: Academic Press, 2001.